JOURNAL OF GEOPHYSICAL RESEARCH, VOL. 112, A08306, doi:10.1029/2006JA012203, 2007



# Thermospheric nitric oxide at higher latitudes: Model calculations with auroral energy input

C. Sætre,[1] C. A. Barth,[2] J. Stadsnes,[1] N. Østgaard,[1] S. M. Bailey,[3] D. N. Baker,[2] G. A. Germany,[4] and J. W. Gjerloev[5]

Received 1 December 2006; revised 11 May 2007; accepted 25 May 2007; published 24 August 2007.

[1] The nitric oxide (NO) density in the lower thermosphere has been calculated by a photochemical model for NOx and compared with measured NO densities from Student Nitric Oxide Explorer (SNOE). At higher latitudes the most important contributor for NO density increases is energetic electron precipitation. The electron energy is estimated in two ways, from auroral ultraviolet (UV) and X-ray measurements obtained from Ultraviolet Imager (UVI) and Polar Ionospheric X-ray Imaging Experiment (PIXIE) on board the Polar satellite and from ground magnetometer measurements. For the time intervals when the Polar satellite was not above the northern hemisphere, a parameterization of the electron energy flux from ground magnetic measurements was used. This parameterization was based on data from the SuperMAG database compared to UVI/PIXIE derived electron energy fluxes. The negative perturbation in the northward ground magnetic component is found to be linearly related to the precipitating electron energy flux. The 4-day period studied is from 30 April (day 120) until 4 May 1998, where the onset of a geomagnetic storm occurred 2 May (day 122). The results of the comparisons show an overall larger modeled nitric oxide density at auroral latitudes than what was measured by SNOE. The largest discrepancies were for the day of the storm onset, when the background atmosphere was more distorted by Joule heating. The next day the agreement between the model and the observations was far better, which might be due to less amount of Joule heating this day.

**Citation:** Sætre, C., C. A. Barth, J. Stadsnes, N. Østgaard, S. M. Bailey, D. N. Baker, G. A. Germany, and J. W. Gjerloev (2007), Thermospheric nitric oxide at higher latitudes: Model calculations with auroral energy input, *J. Geophys. Res.*, *112*, A08306, doi:10.1029/2006JA012203.

## 1. Introduction

[2] Nitric oxide is an important constituent of the upper atmosphere with important properties for radiative cooling and chemical reactions. Since its lifetime in the thermosphere is about 1 day under sunlit conditions, nitric oxide may be used as a tracer of atmospheric motions. There are predictions and observations showing that thermospheric NO can be transported to lower altitudes within a strong polar vortex and react with ozone in the stratosphere [e.g., *Solomon et al.*, 1982; *Randall et al.*, 2005, 2006].

[3] Precipitating energetic particles cause dissociation, ionization, and excitation of the upper atmospheric molecules and atoms. Excited nitrogen atoms, $N(^2D)$, react with molecular oxygen to produce NO. The maximum density of NO is in the lower thermosphere, around 110 km altitude. NO is mainly destroyed by photodissociation from solar far ultraviolet radiation, and the subsequent reaction with ground state nitrogen atoms, $N(^4S)$. Photoelectrons produced from solar soft X rays and extreme ultraviolet radiation (EUV) increase the NO at all latitudes where sunlight is present. The NO density in the lower thermosphere therefore varies with the time of day, the solar radiation, and the auroral particle precipitation. At higher latitudes, auroral precipitation dominates the production of NO.

[4] *Siskind et al.* [1989b] investigated the variation of thermospheric nitric oxide during an auroral storm at low and middle latitudes, where the effect of Joule heating and solar soft X rays were dominant for the production of NO. In a companion paper, *Siskind et al.* [1989a] analyzed the response of NO to auroral particle precipitation during an auroral storm using a time-dependent photochemical NOx model based on the work of *Cleary* [1986]. The history of the particle precipitation including the characteristic energy and energy flux was used as input to the model. These parameters for specific geographic locations were derived

[1]Department of Physics and Technology, University of Bergen, Bergen, Norway.
[2]Laboratory for Atmospheric and Space Physics, University of Colorado, Boulder, Colorado, USA.
[3]Department of Electrical and Computer Engineering, Virginia Polytechnic Institute and State University, Blacksburg, Virginia, USA.
[4]Center for Space Plasma and Aeronomic Research, University of Alabama in Huntsville, Huntsville, Alabama, USA.
[5]Johns Hopkins University Applied Physics Laboratory, Laurel, Maryland, USA.


0148-0227/07/2006JA012203$09.00

from an empirical model of global precipitation patterns constructed from the Television Infrared Observation Satellite (TIROS) and National Oceanic and Atmospheric Administration (NOAA) auroral particle observations [*Foster et al.*, 1986; *Fuller-Rowell and Evans*, 1987].

[5] A revised version of the NOx model was run with solar soft X-ray measurements from the Student Nitric Oxide Explorer (SNOE) as input for the calculation of the photoelectron flux to determine the NO density at lower latitudes [*Barth and Bailey*, 2004]. Comparison of the model results with the NO measured from SNOE showed remarkable agreement at latitudes equatorward of 30° north and south. The photochemical model has also been used to derive the precipitation electron energy flux from NO measurements by SNOE. *Sætre et al.* [2006] compared the energy deposition from thermospheric NO measurements with that derived from time-integrated X-ray bremsstrahlung measurements from Polar Ionospheric X-ray Imaging Experiment (PIXIE). This study found that at higher latitudes the NOx photochemical model underestimated the energy deposition compared to the PIXIE measurements.

[6] In the present work, we calculate the NO density at higher latitudes using the NOx model with both photoelectron and auroral electron energy input. The auroral electron energy flux and characteristic energy are derived not only from PIXIE measurements as in the work of *Sætre et al.* [2006] but also from Ultraviolet Imager (UVI) measurements for the energy range 1 keV to 100 keV. Both UVI and PIXIE on the Polar spacecraft had a global view of the northern auroral oval for ~10 consecutive hours out of each ~18 hour orbit. Since the NO has a lifetime of ~1 day in sunlight, the auroral electron energy input for the NOx model needs to be known continuously throughout an event. For the time intervals without UVI and PIXIE measurements, we use a parameterization of the electron energy flux based on ground magnetometer measurements.

## 2. Instruments and Methods

### 2.1. SNOE NO Observations

[7] Thermospheric nitric oxide was measured using the technique of limb-viewing ultraviolet spectroscopy from a polar orbiting satellite. The characteristics of the satellite orbit and the instrument are described by *Barth et al.* [2003]. The SNOE spacecraft was in a Sun-synchronous orbit with the ascending node at 1030 solar local time (SLT). The nitric oxide was measured along the track of the satellite by observing the fluorescent scattering of solar radiation from the nitric oxide (0,1) gamma band at 237 nm. The density of nitric oxide was determined using the g-factor calculated by *Stevens* [1995] and an inversion of column emission rates to volume densities as described by *Barth et al.* [2003]. The spinning motion of the spacecraft was used to obtain an altitude profile of nitric oxide between 97 and 150 km with an altitude resolution of 3.3 km and a latitude spacing of 5°. The 15 orbits a day were spaced 24° of longitude apart from each other with a time spacing of 96 min.

### 2.2. NOx Model

[8] The model for nitric oxide chemistry used in this study is a revised version of a photochemical model [*Cleary*, 1986; *Siskind et al.*, 1989b, 1989a; *Barth*, 1992] with updated reaction rates and branching ratios [*Bailey et al.*, 2002]. The model is time-dependent and one-dimensional. It includes vertical transport of $N(^4S)$ and NO by eddy and molecular diffusion. This electron transport is calculated using the glow model of *Solomon et al.* [1988] and *Solomon and Abreu* [1989] which includes the energetic electron transport [*Banks and Nagy*, 1970] for both photoelectrons and auroral electrons. The NOx model uses photochemical equilibrium to calculate the vertical profiles of NO, $N(^4S)$, $N(^2D)$, $NO^+$, $O_2^+$, $N_2^+$, $O^+$, and $O^+(^2D)$. The extreme ultraviolet solar flux (20–103 nm) is calculated from the model of *Hinteregger et al.* [1981], with the 10.7 cm solar radio flux as a proxy for the EUV solar activity. The solar soft X-ray irradiance used in the NOx model was measured by SNOE [*Bailey et al.*, 2000]. The photoelectron fluxes used in the model are found to correspond well with measured fluxes [*Solomon et al.*, 2001]. Modeled nitric oxide densities at lower latitudes produced from energetic photoelectrons are found to be in good agreement with measured densities [*Barth and Bailey*, 2004]. The model for the background neutral atmosphere is the NRL Mass Spectrometer, Incoherent Scatter radar Extended model, NRLMSISE-00 [*Picone et al.*, 2002], where daily values of the 10.7 nm solar flux and the 3 hour Ap geomagnetic index are used as proxies for the solar and geomagnetic activity, respectively. The MSIS models are based on a hydrostatic model of *Bates* [1959].

[9] The $N_2$ ionization rate responds directly to the precipitating electron energy input. The NO density increase is an accumulated response of the increased ionization and dissociation. The amount of NO also varies throughout the day as a function of insolation. However, this effect is minimal compared to the response of the auroral electron energy input at higher latitudes.

[10] The NOx model includes chemical and diffusion loss processes of NO. Some of these processes transform NO into other odd nitrogen species. Photodissociation of NO and the following $N(^4S)$ reaction with another NO molecule have the end product $N_2$ and O. The effective lifetime of this process is 19.6 hours [*Minschwaner and Siskind*, 1993].

### 2.3. Electron Precipitation: UVI and PIXIE Auroral Observations

[11] The Ultraviolet Imager (UVI) [*Torr et al.*, 1995] and the Polar Ionospheric X-ray Imaging Experiment (PIXIE) [*Imhof et al.*, 1995] on board the Polar spacecraft measured the auroral signatures of precipitating electrons of ultraviolet emissions and X-ray bremsstrahlung. These measurements provide a global map of the precipitating electrons.

[12] PIXIE was a pinhole camera observing the X-ray bremsstrahlung in the energy range ~3–22 keV. The spatial resolution was ~700 km above the northern hemisphere, where Polar had its apogee in 1998. The data processing of the PIXIE measurements is described by *Østgaard et al.* [1999], and the method for deriving the electron energy spectrum from about 5 to 100 keV from the PIXIE data is described by *Østgaard et al.* [2000, 2001].

[13] UVI observes ultraviolet emissions in the Lyman-Birge-Hopfield (LBH) band. These measurements are separated in the LBH-short and LBH-long bands. LBH-long emissions are proportional to the precipitating electron

energy flux. The difference in absorption by molecular oxygen of the two LBH bands provides information on the average energy of the precipitating electrons. Owing to the wobbling of the pointable pedestal on the Polar satellite, the horizontal resolution of UVI from apogee is degraded from the nominal value of 35 km to approximately 10 times that value in the direction of the wobble. The horizontal resolution perpendicular to the wobble direction is unaffected. The method for deriving the average electron energy and the electron energy flux from the UVI measurements is described by *Germany et al.* [1997, 1998a, 1998b]. The energy range for the electron spectrum derived from UVI is 0.2–25 keV.

[14] The method of deriving the electron energy spectrum from these two different observation techniques is described by *Østgaard et al.* [2001], where the result also has been compared with electron energy spectra from DMSP low-altitude satellite measurements. The combined UVI and PIXIE measurements provide electron energy spectra for the electron energy range 1–100 keV. Electrons with mean energy around 5 keV deposit most of their energy in the altitude region important for NO production (between 100 and 110 km altitude).

[15] For this work we used the electron energy spectra as input in the photochemical NOx model. The spectra for 10 min intervals derived from UVI and PIXIE measurements, were assembled using two parameter Maxwell spectra. The electron energy flux and mean energy were then averaged over 1 hour intervals. Thus the hourly electron precipitation parameters put into the NOx model were averaged Maxwellian fits to six combined UVI and PIXIE 10 min resolution measurements. There were intervals of up to ~10 hours of continuous measurements from UVI and PIXIE for the event studied here.

### 2.4. Electron Precipitation and Geomagnetic Perturbations

[16] Because of the lack of continuous measurements of the electron precipitation, we aimed for using ground magnetometer observations of the geomagnetic perturbations as a proxy for the auroral electron energy input. The main purpose was to obtain a map of the energy input from electron precipitation, persistent over several days, for input in the NOx photochemical model. The neutral particles are not governed by the magnetic and electric fields. They corotate with the Earth. Hence the coordinate system used in this comparison is geographical.

[17] The geomagnetic disturbances in the north (MAG) magnetic component ($\Delta$N) at higher latitudes are connected to ionospheric currents known as the electrojets. The westward electrojet, giving a negative deflection in $\Delta$N, is related to the Hall conductance, which again is connected to the energetic electron precipitation [e.g., *Baumjohann and Kamide*, 1984; *Ahn et al.*, 1999; *Gjerloev and Hoffmann*, 2001; *Østgaard et al.*, 2002]. The eastward electrojet is thought to be more strongly governed by the electric field [*Baumjohann and Kamide*, 1984; *Ahn et al.*, 1999; *Gjerloev and Hoffmann*, 2001]. Thus for this work we correlate the maximum negative perturbation of the local north magnetic component, $\Delta N < 0$, from the ground-based measurements, with the precipitating electron energy flux derived from UVI and PIXIE observations. Previous studies of geomagnetic indices and their connections to electron precipitation have mainly been focused on the global AE indices [e.g., *Gjerloev and Hoffmann*, 2001; *Østgaard et al.*, 2002]. Here we apply ground magnetometer data from the SuperMAG database, which consists of more than 100 stations located at higher northern latitudes. The comparisons between $\Delta$N and precipitating electron energy flux were made within longitude sectors of 24°.

[18] A two parameter Maxwell electron energy spectrum is derived from UVI and PIXIE measurements for consecutive 10 min intervals. Then the hourly mean of the electron energy flux averaged over a 20° latitude band (50°–70°N) around the auroral oval is compared to the hourly mean of the $\Delta N < 0$ values for the concurrent longitudinal sector. As mentioned above, the $\Delta$N ground perturbations are connected to the Hall conductivity, which again is related to the electron precipitation. The electron energies contributing to the Hall conductance are above ~3 keV. The electron energy flux used in these comparisons is just for the energy range 3–100 keV, the electron precipitation assumed to give changes in the $\Delta N < 0$ ground geomagnetic field.

[19] The global magnetometer network, SuperMAG, is a data set provided by more than 200 ground magnetometer stations [*Gjerloev et al.*, 2004]. This network gives good global coverage and continuous measurements of the ground geomagnetic perturbations. The magnetometer data has a common baseline removal technique, the same time resolution, and the same coordinate system. In the present study, only the stations for the northern hemisphere are used, in all more than 100 stations. However, there are areas like Siberia where there might only be one or two stations available within a 24° longitude sector. The $\Delta$N perturbations in these sectors for the four events investigated here were more often showing high values at high auroral activity than no deflection. Thus we chose to include all longitude sectors in our comparisons. The stations are mainly conveniently located in close proximity to the auroral oval. In the sectors where the number of stations are few, the stations also have relatively good longitudinal coverage.

[20] The comparisons for all the 4 days, for all sectors and all hours of UVI and PIXIE measurements, are gathered in one scatterplot, Figure 1. The correlation of the data sets is 0.75. We assume there is overall no essential electron precipitation when $\Delta N = 0$. The linear fit of the comparisons is calculated using the least squares method. The standard deviation of the residuals is 1.5 [mW/m$^2$].

[21] The comparisons were done for all hours where UVI and PIXIE were measuring, also for times and areas with low activity. Areas outside the UVI and PIXIE's field of views were of course not included. To understand more of the details behind the spreading of the data points in Figure 1, we have plotted the hourly means of the periods with $\Delta N < 0$ and the electron energy flux as functions of universal time. Figure 2 is an example of a well-correlated high-activity event, 216°–240°E, day 122 of 1998. The black histogram is the hourly mean $\Delta N < 0$ for the region, and the grey histogram is the hourly mean electron energy flux derived from UVI/PIXIE. The maximum activity was ~2 hours after midnight for this sector. Overall, the night sector shows a fairly good correlation between the two data sets.

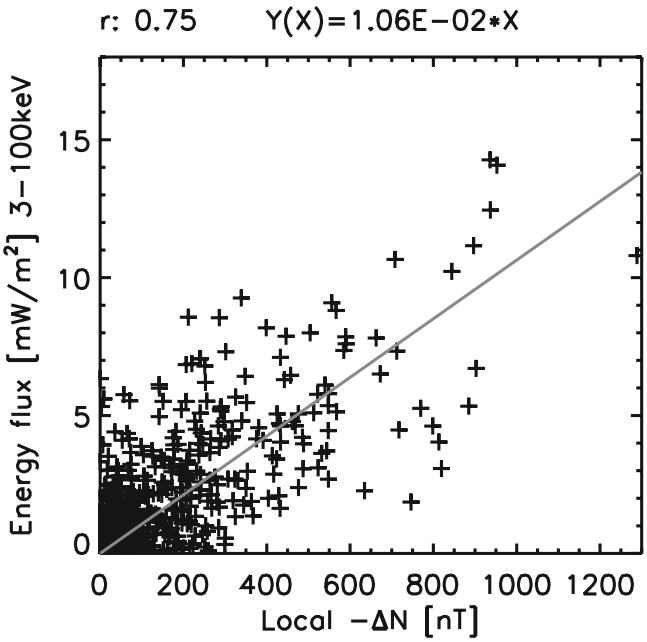


**Figure 1.** Precipitating electron (3–100 keV) energy flux averaged over a 20° auroral latitude band, plotted against the maximum negative perturbation of the ground geomagnetic north component, $\Delta N < 0$. The values are hourly means, within 24° geographic longitude sectors, for days 120, 122, 123, and 177 of 1998. There are 589 points in total, most of them at low values. The correlation coefficient is 0.75. The linear fit has a slope of 0.0106 [mW m$^{-2}$ nT$^{-1}$] with a standard deviation of 0.0002. The standard deviation for the residuals is 1.5 [mW/m$^2$].

Sometimes, though, the electron energy flux implies a quite larger activity than the ground magnetometer data. Such an example is shown in Figure 3. There are 14 geomagnetic stations for this sector, so one would assume that this was sufficient for registering any ionospheric current above the region. Eleven of the stations are, however, part of the magnetometer array at the west coast of Greenland. If the currents related to the auroral activity were located quite south of these stations, a much fainter deflection would be registered. A situation where the geomagnetic $\Delta N < 0$ perturbations gave relatively larger values than the electron energy flux derived from UVI and PIXIE, is displayed in Figure 4, from local time ~4 (corresponding to 1000 UT in Figure 4) and onward. The field of views for UVI and PIXIE were quite good for this longitude sector and time interval. The first 5 hours of the event, where the actual longitude interval was in the local midnight to early morning sector, the correlation was exceptionally good. On the nightside the ionospheric current systems are believed to be controlled by the Hall conductance [e.g., *Kamide and Vickrey*, 1983; *Sugino et al.*, 2002; *Gjerloev and Hoffmann*, 2001]. In the morning sector, however, the currents can be more influenced by the electric field [*Kamide and Kokubun*, 1996; *Gjerloev and Hoffmann*, 2001]. Thus the relative larger amplitudes of the $\Delta N < 0$ perturbations in the later part of the morning sector were probably caused by an increased convectional electric field and were not directly related to the electron precipitation through increased Hall conductance.

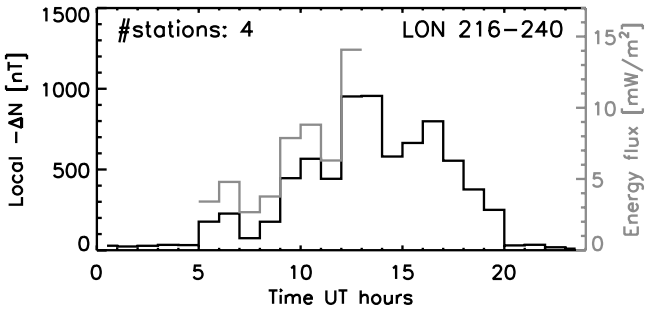


**Figure 2.** Hourly mean of the negative ground north geomagnetic perturbation, $\Delta N < 0$ (black, units of nT). Electron energy flux (3–100 keV) derived from UVI and PIXIE observations, hourly mean averaged over 20° auroral latitude band (gray, units of mW m$^{-2}$). Both data sets are within geographic longitude sector 216°–240°E, day 122 of 1998, and are plotted as functions of universal time. The number of stations used to get the $\Delta N < 0$ values within this 24° longitude sector is indicated in the upper left corner.

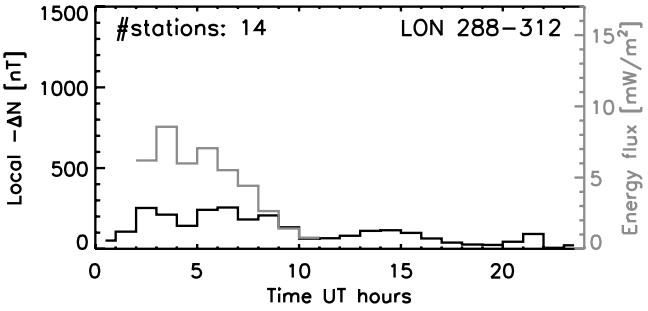


**Figure 3.** Same type of plot as Figure 2, for 288°–312°E, day 177 of 1998.

[22] To summarize, the comparisons between hourly mean of $\Delta N < 0$ perturbations from ground magnetometer data and energetic electron energy flux from UVI and PIXIE observations for geographical longitude sectors gave a correlation of 0.75. We find this result significant and conclude that ground $\Delta N < 0$ perturbations may be used together with UVI and PIXIE data to provide geographical maps of the energetic electron precipitation which are continuous in time. The uncertainties of the parameteriza-

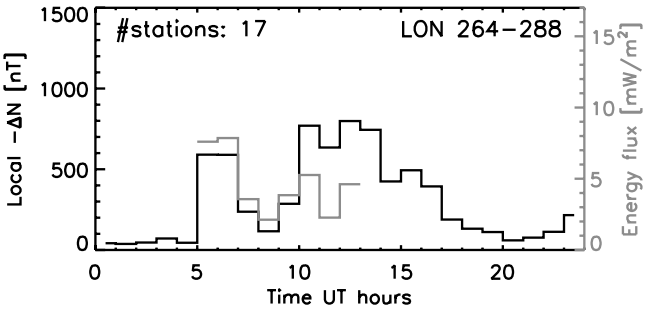


**Figure 4.** Same type of plot as Figure 2, for 264°–288°E, day 122 of 1998.

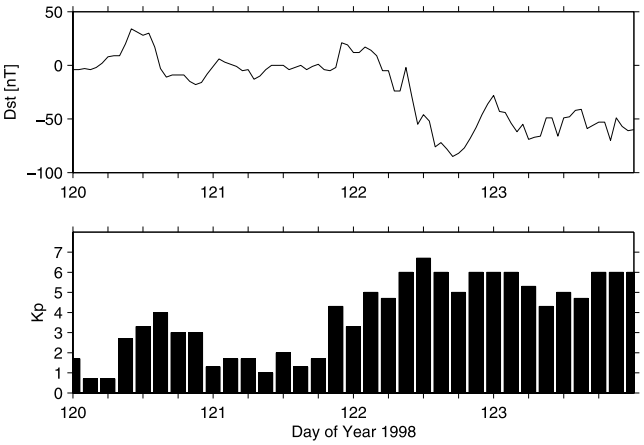


**Figure 5.** Dst and Kp index for days 120 to 123 of 1998.

tion concerning local time fluctuations are not believed to give a systematic bias for the model calculations done for several consecutive hours (∼8 hours and more). A characteristic energy of 4 keV was chosen for use with the energy flux derived from the magnetometer data. This is approximately the mean characteristic energy calculated from the PIXIE and UVI data for the times when that data was available.

## 3. Results NOx Model

[23] The NOx model calculated the nitric oxide density in 24° longitude times 5° latitude boxes. The input parameters were the average auroral electron energy flux and characteristic energy, for the same geographical areas, in 1 hour intervals. The modeled NO density was compared to that measured by SNOE. The comparisons were done as functions of universal time, latitude, altitude, and solar local time for specific longitude intervals for each SNOE orbit.

[24] The event presented here is from day 120 to day 123 of 1998. Figure 5 gives the Dst and Kp geomagnetic activity indices for these days. The onset of the geomagnetic storm was between 0500 and 0600 UT on day 122. In Figure 6 the NO density from the model (black curve) and the NO density from SNOE measurements (blue curve), at 110 km altitude, are plotted as functions of universal time from day 120 until day 124 of 1998. The four latitude sectors between 50°N and 70°N are displayed. The time resolution for this plot is ∼1.5 hours (distance between the dots), which is the time between the SNOE orbits. The location in longitude varies with 24 degrees for each of these time steps and the NO density shown is a mixture of temporal and spatial changes. Since the SNOE satellite was in a Sun-synchronous orbit, the NO measurements were done at the same local time from one orbit to the next. The plot gives the overall variations in nitric oxide in the lower thermosphere during the course of the geomagnetic storm. Also shown is the total auroral electron energy flux for the preceding 16 hours (from 1800 SLT the previous day to 1000 SLT, the time sector where we assume the main electron precipitation occurred) for the particular regions compared (red histogram). The energy fluxes are derived directly from UVI/PIXIE measurements, and for the hours when UVI/PIXIE did not cover the northern auroral oval, from the magnetic perturbation parameterization. Each column of the energy flux histogram consists of the sum of auroral activity for the particular longitude region for the evening, night, and morning hours before the SNOE measurements for the region.

[25] The first day of comparisons, 120, the model has not had time to respond to the energy input and we focus on the comparisons for the next 3 days, 121, 122, and 123 of 1998. On day 121 the geomagnetic activity was low. There was, however, some electron precipitation at latitude bands 50–55°N and 55–60°N that produced a small increase in the observed nitric oxide density. The NOx model calculation matched this increase very nicely. There was additional electron precipitation at latitude bands 60–65°N and 65–70°N that caused the NOx model to predict an increase in nitric oxide density that was not reflected in the NO measurements from SNOE.

[26] The next day, 122, where the onset of the geomagnetic storm occurred ∼0530 UT, there was a rather good correspondence between the two density profiles prior to the storm. From ∼1200 to 1500 UT for the three most northerly sectors, there was a decrease in the measured NO density, while there was a profound activity measured by UVI and PIXIE for these regions. After ∼1500 UT the measured density increased strongly in accordance with the auroral electron energy input to the model. However, the magnitude of the measured NO density was substantially less, by a factor 2–4, than the modeled density. During the last hours of day 122 and the first hours of day 123, the measured NO density was actually enhanced while the modeled NO density decreased. This also occurred the last hours of day 123.

[27] On day 123 there were four orbits during the first half of the day where there were no SNOE measurements. During the second half of the day, the agreement between the model calculations and the observations improved. In latitude bands 60–65°N and 65–70°N, there was a decrease in measured NO density compared to the model result between ∼1330 and 1500 UT. During the following couple of hours the measured density increased showing a good agreement with the auroral energy observations. When interpreting these changes in nitric oxide as function of universal time, it is important to remember that the longitude sectors are not the same from one measurement time to another.

[28] Figure 7 shows the NO density variations as function of solar local time for one of the longitude sectors (276°E) on day 122 at higher latitudes that experienced a clear reduction of the measured NO density. This reduction was not expected, since the UVI and PIXIE data clearly showed an input of auroral electron energy for this region, as shown by the relatively high $N_2$ auroral ionization rate in Figure 7 (gray histogram). The corresponding universal time for the SNOE measurements for this longitude sector was ∼1500 UT. Figure 7 gives the modeled NO density at 106 km altitude (black solid curve) as a function of solar local time. Also shown is the measured NO density as squares, one measurement for the specific longitude sector for each day. The nitric oxide photodissociation rate (dotted line) and the $N_2$ auroral ionization rate (gray histogram) are both plotted on an arbitrary scale. The auroral ionization rate is directly

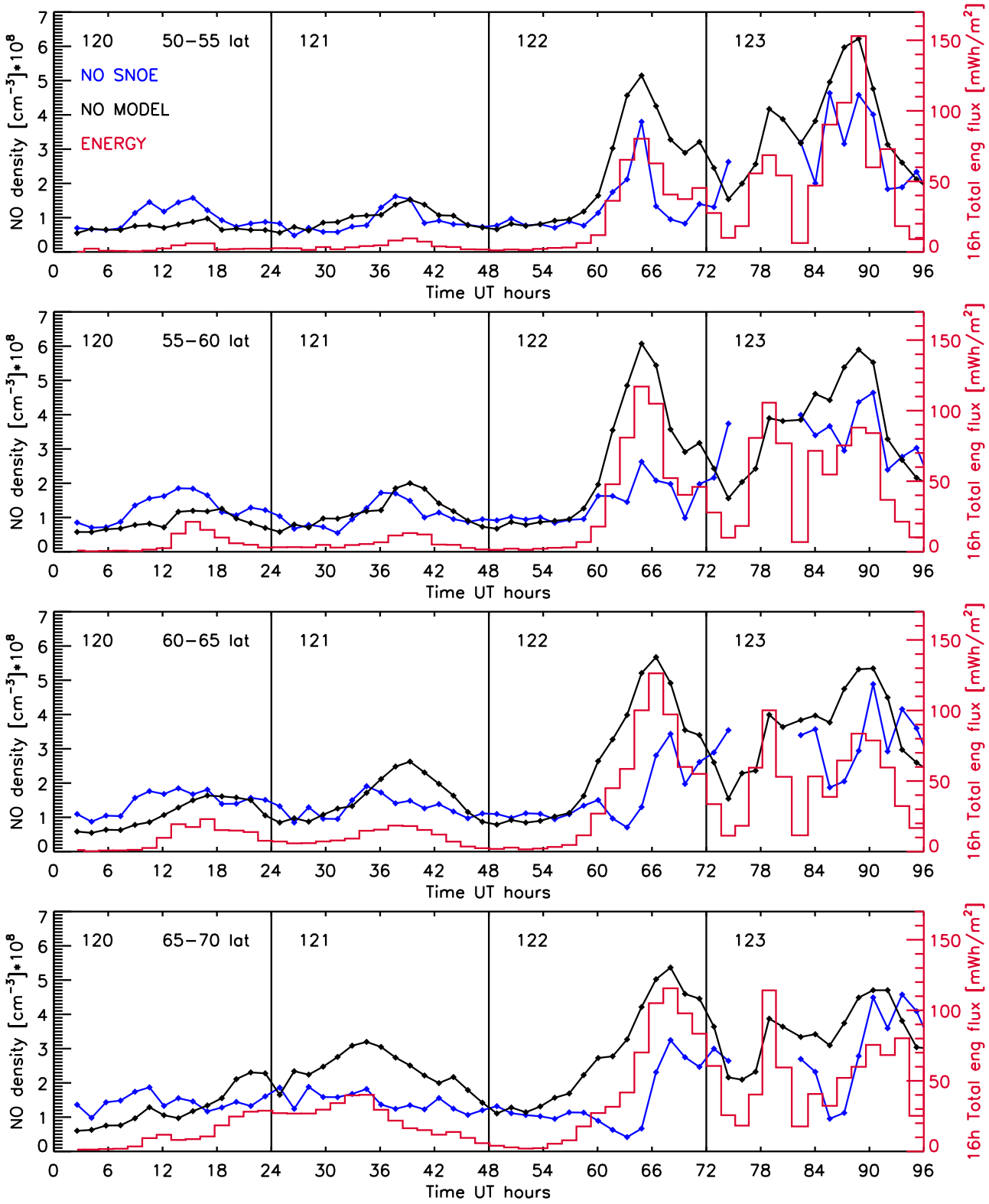


**Figure 6.** Nitric oxide density [molecules/cm$^3$] at 110 km altitude as function of universal time for the days 120 to 123 of 1998. The black curve is the modeled NO density, and the blue curve is the NO density measured by SNOE. The red histogram displays the total electron energy flux [mWh/m$^2$] the preceding night and morning (16 hours) for each of the longitude sectors of the SNOE dayside measurements. Each of the days, SNOE orbit number 1 between 120° and 144°E, occurred at ~0030 UT. The satellite passes then moved westward. The orbit number 6 for longitudes 336°–360°E, was at ~1030 UT. And finally, orbit number 15, 144°–168°E, occurred at ~2300 UT. The steps between each orbit was 24° longitude, in the westward direction.

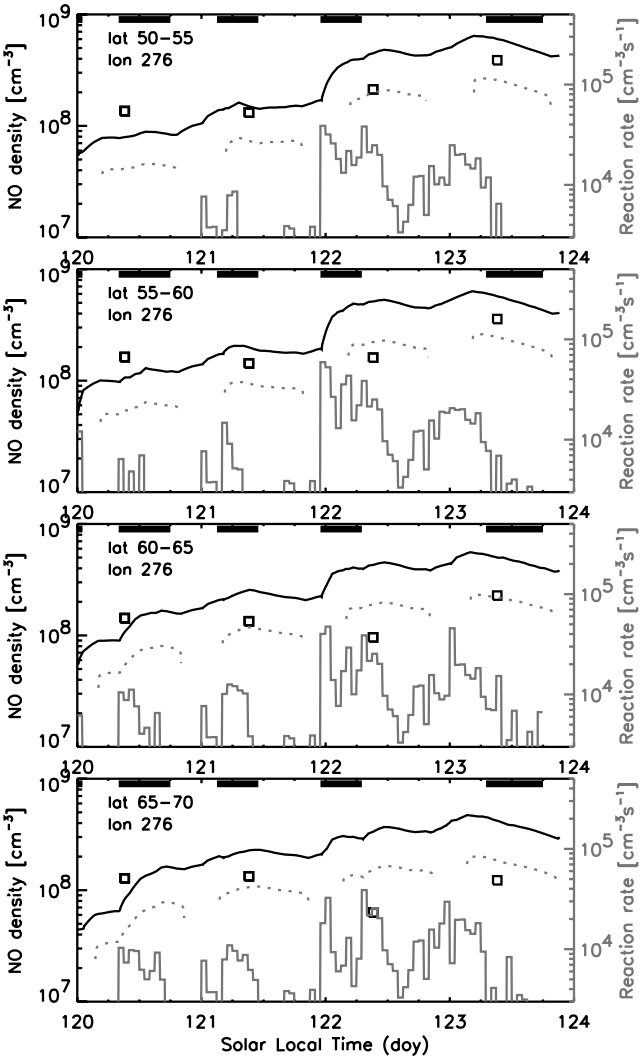


**Figure 7.** Solar local time variations of the NOx model calculations at 106 km altitude for the days 120 to 123 of 1998, four latitude sectors around 276° east. The solid black line is the NO density calculated from the NOx model. The squares are the NO density measured by SNOE for the particular region. The gray histogram displays the $N_2$ auroral ionization rate, and the gray dotted line is the NO photodissociation rate (times 25 to fit in scale). The thick lines in the top of each plot indicate the time intervals for the UVI and PIXIE measurements.

related to the input precipitation electron energy flux from the UVI and PIXIE measurements and the SuperMAG parameterization. The parameterization was averaged over all the four latitude sectors, and hence the hours where UVI and PIXIE had no observations, the energy flux was the same for all the latitude sectors. For the example given in Figure 7, we see that for the two lowest latitudes there was a fairly good agreement between the model and the SNOE data for day 121. The modeled NO density for the next day, 122, showed a significantly larger increase than the measured density. For the two upper latitude sectors the measured NO density at 106 km altitude actually decreased substantially from day 121 to day 122, in spite of the observed auroral activity at these latitudes. For all latitudes there was a clear increase in the measured NO density from day 122 to day 123. However, it seems like the model basis on day 122 was too high compared to the measurements to give a good agreement between the two profiles on day 123 either. Clearly, something happened on day 122 that strongly suppressed the effect on nitric oxide from auroral electron precipitation.

[29] Figure 8 gives an example of how the modeled NO density is larger than the measured NO density for all the 4 days. The factor between the model result and the measured density seems to remain the same throughout the entire period. This case is for 204°E, 60°–65°N, corresponding to ~2000 UT for the SNOE measurements. Unlike the example given in Figure 7, the SNOE observations show a clear increase of the NO density on day 122 due to the geomagnetic storm.

[30] The altitude profiles of the nitric oxide densities for 228°E for all the four latitude sectors for day 122 (upper) and day 123 (lower) of 1998, are shown in Figure 9. The universal time for the SNOE measurements at this longitude was ~1800 UT. The modeled nitric oxide density on day 122 was overall larger than that measured by SNOE. This was especially evident at altitudes above ~120 km. The auroral electron energy flux used as input for the model was not particularly large for this longitude sector during either of these days. We see that on day 122, the model displays none of the structures of the measured NO profile above ~120 km altitude. The nitric oxide altitude profiles were better correlated at all altitudes on day 123. A few of the cases with the most evident differences between the model and the measured NO density for day 123 had a much larger difference the day before (day 122).

## 4. Discussion

[31] The objective for this study was to validate the calculation of lower thermospheric nitric oxide at higher latitudes by a photochemical model [*Barth*, 1992; *Bailey et al.*, 2002]. Previous work with the same model gave good agreement with observed nitric oxide densities at low latitudes where the effect of electron impact on the production of nitric oxide is from photoelectrons which are produced by the action of solar soft X rays on molecular nitrogen and atomic oxygen.

[32] The results from this study show that the photochemical model overestimates, to a varying degree, the nitric

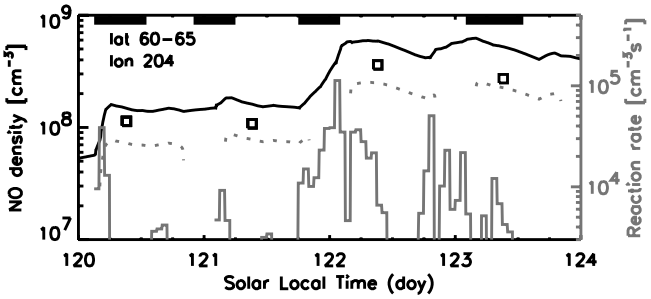


**Figure 8.** Same type of plot as Figure 7, for 204° east and 60–65° north.

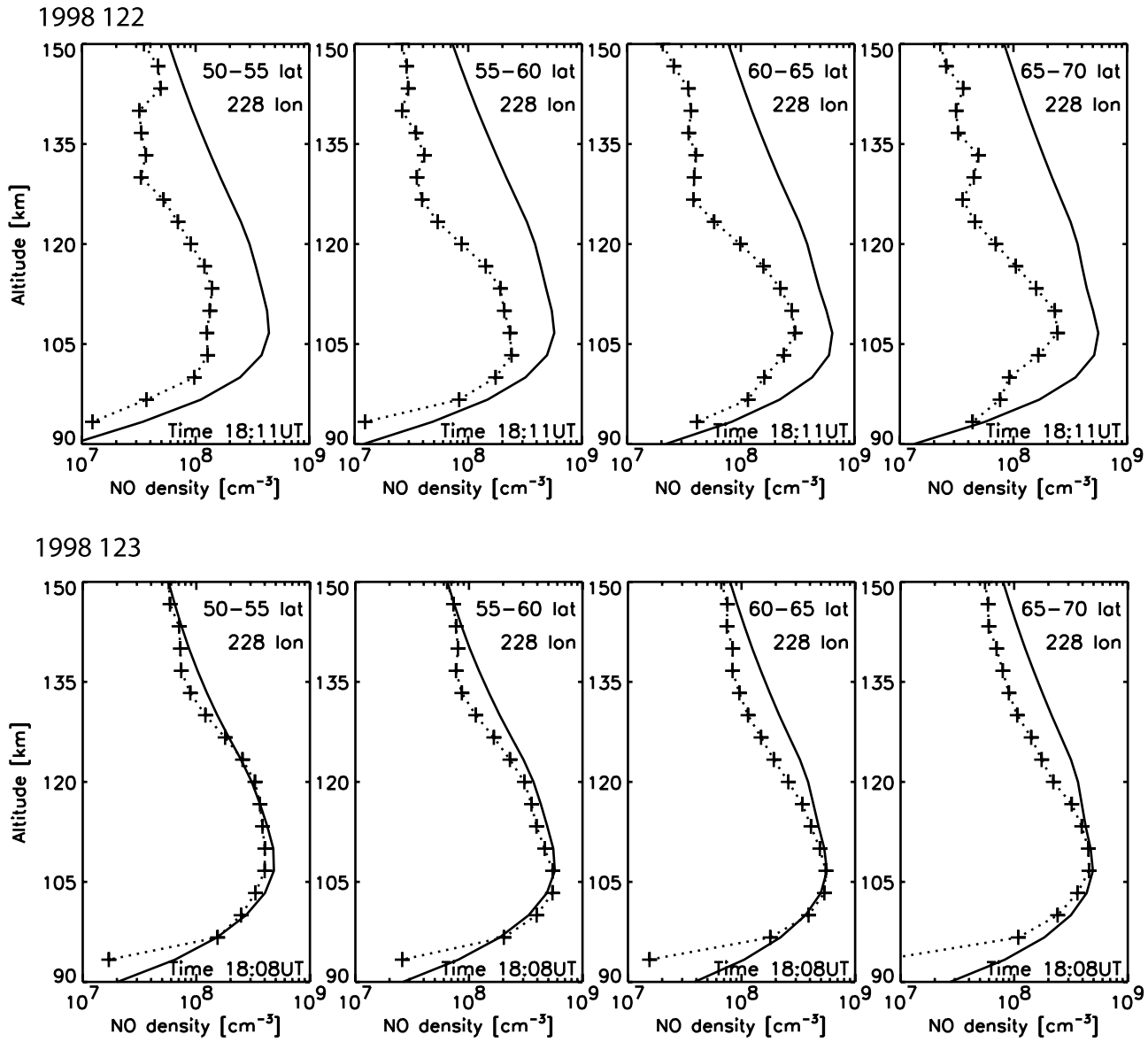


**Figure 9.** NO density at 228° east, four latitude regions, as measured by SNOE (dotted line with crosses) and calculated from the NOx model (solid line). The upper four plots are for day 122, and the lower four plots are the same regions for day 123. The universal time for the SNOE measurements at 60°N are given in the lower right corner of each plot.

oxide density in the lower thermosphere during geomagnetic active periods. The work of *Siskind et al.* [1989a] was based on this same photochemical model and had as input for the auroral electron energy deposition the hemispherical power index from the NOAA measurements and a statistical model for the auroral precipitation pattern. Their model calculations gave a far greater NO density at higher latitudes than that measured by the Solar Mesosphere Explorer (SME). From the UVI and PIXIE measurements we get the structure and time history of the electron precipitation, without having to use a statistical model. Our results show that the model results exceed the SNOE data by a factor of 2–4 for the day of the storm onset (see Figure 9, top). The good correlation for the lower latitudes in the previous study by *Barth and Bailey* [2004], also indicates that the revised $N(^2D)$ yield provides a more correct estimate of the nitric oxide production. The results of the present study, are substantially better for the day after the storm onset (123), when the atmosphere experienced less heating (see Figure 9, bottom). This was also the case for another event, not presented here, for days 176 to 178, 1998.

[33] The discrepancies between the modeled NO density and the measurements might in part be due to the electron energy input to the model being wrong. On the basis of the good correlation on lower latitudes [*Barth and Bailey*, 2004], we believe that the method for the photoelectrons produced by solar soft X rays and extreme ultraviolet to be quite satisfactory also for the higher latitudes. Also for the results in this study, the modeled NO density agreed well with the observations when the auroral electron energy

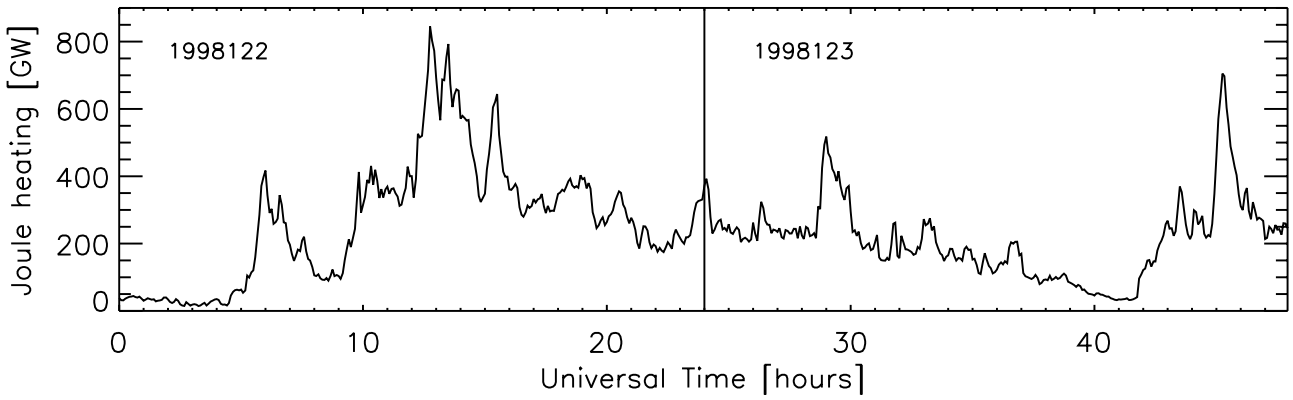


**Figure 10.** Joule heating derived from the AMIE procedure for days 122 and 123 of 1998.

input was low. That is, the difference was less than ~50%. The auroral electron energy input for the model was mainly from UVI and PIXIE. For continuity of the energy input the electron energy flux was also derived from ground geomagnetic measurements from the SuperMAG database, in the time intervals without UVI and PIXIE measurements. The electron energy parameters were derived from the UVI and PIXIE measurements by using two different techniques and then matched together to form one electron energy spectrum. We consider these results to be a satisfactory measure of the mean electron energy deposition into the lower thermosphere per hour. This hourly auroral electron energy input for the model was based on (usually) six energy spectra derived from UVI and PIXIE measurements. It is difficult to give an exact value for the uncertainty of this auroral electron energy flux and characteristic energy. There are no signs that they might be systematically overestimated, according to previous work where this method was used [*Østgaard et al.*, 2000].

[34] The SuperMAG parameterization was divided in 24° longitude sectors. The linear relation between the energy flux derived from UVI and PIXIE measurements and the $\Delta N < 0$ perturbation of the geomagnetic field, had a correlation of 0.75. There were longitude sectors where the number of magnetometer stations was quite low, especially in Siberia. The derived energy flux in these regions might be underestimated. This could be the reason for the differences in the model NO density and the measured one on the night (~0300 UT) of day 123 and on the evening (~2100–2400 UT) on day 123. Here the SNOE measurements of NO showed an increase, while the modeled density was decreasing. For the regions at hand, the main electron input was derived from magnetometer data, and the sectors had few stations. For the other longitude regions, there were no systematic variations of the nitric oxide model results whether the input was from UVI and PIXIE or from the magnetometer data.

[35] The fixed electron characteristic energy at 4 keV for the SuperMAG parameterization could also cause some discrepancy. However, the altitude profiles of NO seem to be more governed by the neutral wind transport due to temperature gradients [e.g., *Price et al.*, 1995]. The height of the maximum NO density was not particularly different for the modeled and the measured profile. The characteristic energy of the auroral electrons, and hence the altitude of the maximum energy deposition, seemed to be well described by both the UVI and PIXIE measurements and the fixed 4 keV value for the SuperMAG events.

[36] The nitric oxide densities from SNOE dayglow measurements had a total uncertainty of about 20% [*Barth and Bailey*, 2004]. When also considering the good results between the photochemical model calculations and the measured NO density at low latitudes where photoelectrons are the source of the electron impact reactions [*Barth and Bailey*, 2004], neither the SNOE NO measurements nor the SNOE solar soft X-ray observations should give the large discrepancies at higher latitudes.

[37] The differences between the model and the measurements were more dominant on day 122 than on day 123. This was especially evident in the altitude profiles of the NO density (Figure 9). One of the main differences between these 2 days was the amount of Joule heating. Figure 10 shows the amount of Joule heating derived from the Assimilative Mapping of Ionospheric Electrodynamics (AMIE) procedure for days 122 and 123 [*Richmond et al.*, 1992]. On day 122 the overall Joule heating after the onset of the geomagnetic storm was larger than on day 123. On day 122 the global Joule heating exceeded 300 GW for about 10 hours. This is considered to be a moderate amount of heating. On day 123 it was above 300 GW for only ~4 hours in total. During periods of significant Joule heating, the atmosphere at auroral latitudes will expand, enhancing the neutral winds. The model for the background atmosphere used here, NRLMSISE-00, is based on the *Bates* [1959] description. For periods when there is substantial Joule heating this description is not applicable. Hence the NRLMSISE-00 model will not be sufficient for modeling the correct response of the atmosphere. The heating on day 122 was considerable enough that the atmosphere did not follow the *Bates* [1959] formulism, and the NO observations could therefore not be modeled correctly by the NOx model with the NRLMSISE-00 estimation for the background atmosphere. For the lower and middle latitudes the atmosphere was not affected to that extent by the amount of Joule and particle heating. The results of this study are hence not in conflict with the previous high correlation results for the tropics [*Barth and Bailey*, 2004]. The better correlations on day 123 show that

when the effect of the Joule heating is not as dominant, the NOx model works much better.

## 5. Summary and Conclusion

[38] The auroral electron energy has been derived from UVI and PIXIE measurements of auroral UV emissions and X-ray bremsstrahlung. For the times when the two instruments were not measuring the northern auroral oval, the electron energy flux was estimated from ground geomagnetic measurements. The auroral electron energy was arranged in geographical boxes of 5° latitude and 24° longitude sectors. It was continuous in time over 4 days, from day 120 until day 124 of 1998. This period covered the onset of a geomagnetic storm on the morning of day 122. The auroral electron energy was used as the input to a photochemical model for nitric oxide. The energy input from photoelectrons was also accounted for. The modeled NO density in the lower thermosphere between latitudes 50° and 70°N was compared with the NO density measured by SNOE for the same geographical area. The model calculations show good agreement with the measured NO density for the time prior to the storm onset, that is day 121 and the beginning of day 122. Also on the day after the storm main phase, day 123, the comparisons are good. For these time intervals the modeled nitric oxide is generally well within a factor of two of the measured density at all altitudes. For some longitude sectors the agreement is very good, as shown in the example in Figure 9 for day 123. On the day of the storm, day 122, the model calculations were up to a factor of four larger than the SNOE measurements. Previous comparisons of modeled NO density with auroral electron energy input [*Siskind et al.*, 1989a] with revised NO data from the SME satellite [*Siskind et al.*, 1998] also showed a factor 3–4 overestimate for the model result at higher latitudes during high auroral activity. The Joule heating effects on the background atmosphere, and the resulting increase of the neutral winds, were not included in the one-dimensional nitric oxide model used here. We suggest that increased transport of NO due to significant Joule heating on the day of the storm might cause severe loss of NO and thus explain the relatively higher discrepancy between model and observed NO densities for this day. The day after, when the Joule heating was not as severe, the agreement between the modeled and measured NO densities was better. The reactions involved in the model, and their reaction rates and branching ratios, are probably sufficiently accurate to calculate the chemical production and loss of nitric oxide in the lower thermosphere. It is, however, necessary to incorporate the transport of the neutral gases, especially for events with significant atmospheric heating.

[39] To conclude, the photochemical model for NO, with NRLMSISE-00 as the model for the background atmosphere, is unable to calculate precisely the correct NO density in the lower thermosphere without incorporating significant transport effects. On the basis of the good agreement between the modeled nitric oxide density and the measurements before and after the geomagnetic storm, we believe that the chemical processes of the NOx model are a correct description of the nitric oxide production and loss in the auroral region.

[40] **Acknowledgments.** The Norwegian authors thank the Research Council of Norway for financial support. For the ground magnetometer data we gratefully acknowledge: the S-RAMP Database, PI K. Yumoto and K. Shiokawa; the SPIDR database; Intermagnet; the institutes who maintain the IMAGE magnetometer array; AARI data, PI Oleg Troshichev; Danish Meteorological Institute, Ole Rasmussen and Project Scientist Jurgen Watermann; the CARISMA, PI Ian Mann; the MACCS program, PIs W. J. Hughes and M. Engebretson as well as the Geomagnetism Unit of the Geological Survey of Canada; GIMA, PI John Olson; MEASURE, UCLA IGPP and Florida Institute of Technology; USGS, Jeffrey J. Love; MAGIC, PI C. Robert Clauer; SAMBA, PI Eftyhia Zesta; 210 Chain, PI K. Yumoto; SAMNET, PI Farideh Honary; IMAGE, PI Ari Viljanen. We thank WDC for Geomagnetism Kyoto geomagnetic index service and NOAA's National Geophysical Data Center, the stations and the persons who derive the Dst and Kp indices. We also thank Gang Lu for Joule heating data from the AMIE model.

[41] Zuyin Pu thanks the reviewers for their assistance in evaluating this paper.

## References

Ahn, B. H., B. A. Emery, H. W. Kroehl, and Y. Kamide (1999), Climatological characteristics of the auroral ionosphere in terms of electric field and ionospheric conductance, *J. Geophys. Res.*, *104*, 10,031.

Bailey, S. M., T. N. Woods, C. A. Barth, S. C. Solomon, L. R. Canfield, and R. Korde (2000), Measurements of the solar soft x-ray irradiance by the Student Nitric Oxide Explorer: First analysis and underflight calibrations, *J. Geophys. Res.*, *105*, 27,179.

Bailey, S. M., C. A. Barth, and S. C. Solomon (2002), A model of nitric oxide in the lower thermosphere, *J. Geophys. Res.*, *107*(A8), 1205, doi:10.1029/2001JA000258.

Banks, P. M., and A. F. Nagy (1970), Concerning the influence of elastic scattering upon photoelectron transport and escape, *J. Geophys. Res.*, *75*, 1902.

Barth, C. (1992), Nitric oxide in the lower thermosphere, *Planet. Space Sci.*, *40*, 315.

Barth, C. A., and S. M. Bailey (2004), Comparison of a thermospheric photochemical model with Student Nitric Oxide Explorer (SNOE) observations of nitric oxide, *J. Geophys. Res.*, *109*, A03304, doi:10.1029/2003JA010227.

Barth, C. A., K. D. Mankoff, S. M. Bailey, and S. C. Solomon (2003), Global observations of nitric oxide in the thermosphere, *J. Geophys. Res.*, *108*(A1), 1027, doi:10.1029/2002JA009458.

Bates, D. R. (1959), Some problems concerning the terrestrial atmosphere above about the 100 km level, *Proc. R. Soc. London, Ser. A*, *253*, 451.

Baumjohann, W., and Y. Kamide (1984), Hemispherical Joule heating and the AE indices, *J. Geophys. Res.*, *89*, 383.

Cleary, R. J. (1986), Daytime high-latitude rocket observations of the NO $\gamma$, $\delta$ and $\varepsilon$ bands, *J. Geophys. Res.*, *91*, 11,337.

Foster, J. C., J. M. Holt, R. G. Musgrove, and D. S. Evans (1986), Ionospheric convection associated with discrete levels of particle precipitation, *Geophys. Res. Lett.*, *13*, 656.

Fuller-Rowell, T. J., and D. S. Evans (1987), Height-integrated Pedersen and Hall conductivity patterns inferred from the TIROS-NOAA satellite data, *J. Geophys. Res.*, *92*, 7606.

Germany, G. A., G. K. Parks, M. J. Brittnacher, J. Cumnock, D. Lummerzheim, J. F. Spann, L. Chen, P. G. Richards, and F. J. Rich (1997), Remote determination of auroral energy characteristics during substorm activity, *Geophys. Res. Lett.*, *24*, 995.

Germany, G. A., G. K. Parks, M. J. Brittnacher, J. F. Spann, J. Cumnock, D. Lummerzheim, F. J. Rich, and P. G. Richards (1998a), Energy characterization of a dynamic auroral event using GGS UVI images, in *Geospace Mass and Energy Flow: Results From the International Solar-Terrestrial Physic Program*, *Geophys. Monogr. Ser.*, vol. 104, edited by J. L. Horwitz, D. L. Gallagher, and W. K. Peterson, p. 143, AGU, Washington, D. C.

Germany, G. A., J. F. Spann, G. K. Parks, M. J. Brittnacher, R. Elsen, L. Chen, D. Lummerzheim, and M. H. Rees (1998b), Auroral observations from the Polar Ultraviolet Imager (UVI), in *Geospace Mass and Energy Flow: Results From the International Solar-Terrestrial Physic Program*, *Geophys. Monogr. Ser.*, vol. 104, edited by J. L. Horwitz, D. L. Gallagher, and W. K. Peterson, p. 149, AGU, Washington, D. C.

Gjerloev, J. W., and R. A. Hoffmann (2001), The convection electric field in auroral substorms, *J. Geophys. Res.*, *106*, 12,919.

Gjerloev, J. W., M. Friel, R. A. Hoffman, K. Takahashi, R. Barnes, C. Meng, and R. A. Greenwald (2004), The global magnetometer network initiative: SuperMAG, *Eos Trans. AGU*, *85*(47), Fall Meet. Suppl., Abstract SH41A-1079.

Hinteregger, H. E., K. Fukui, and B. R. Gilson (1981), Observational, reference, and model data on solar EUV, from measurements on AE-E, *Geophys. Res. Lett.*, *8*, 1147.

Imhof, W. L., et al. (1995), The Polar Ionospheric X-ray Imaging Experiment (PIXIE), *Space Sci. Rev.*, *71*, 385.

Kamide, Y., and S. Kokubun (1996), Two-component auroral electrojet: Importance for substorm studies, *J. Geophys. Res.*, *101*, 13,027.

Kamide, Y., and J. F. Vickrey (1983), Relative contribution of ionospheric conductivity and electric field to the auroral electrojets, *J. Geophys. Res.*, *88*, 7989.

Minschwaner, K., and D. E. Siskind (1993), A new calculation of nitric oxide photolysis in the stratosphere, mesosphere, and lower thermosphere, *J. Geophys. Res.*, *98*, 20,401.

Østgaard, N., J. Bjordal, J. Stadsnes, and E. Thorsen (1999), PIXIE data processing at the University of Bergen, *Tech. Rep. 1999-05*, Dept. of Physics, Univ. of Bergen, Bergen, Norway.

Østgaard, N., J. Stadsnes, J. Bjordal, R. R. Vondrak, S. A. Cummer, D. L. Chenette, M. Schulz, and J. G. Pronko (2000), Cause of the localized maximum of x-ray emission in the morning sector: A comparison with electron measurements, *J. Geophys. Res.*, *105*, 20,869.

Østgaard, N., J. Stadsnes, J. Bjordal, G. A. Germany, R. R. Vondrak, G. K. Parks, S. A. Cummer, D. L. Chenette, and J. G. Pronko (2001), Auroral electron distributions derived from combined UV and X-ray emissions, *J. Geophys. Res.*, *106*, 26,081.

Østgaard, N., R. R. Vondrak, J. W. Gjerloev, and G. Germany (2002), A relation between the energy deposition by electron precipitation and geomagnetic indices during substorms, *J. Geophys. Res.*, *107*(A9), 1246, doi:10.1029/2001JA002003.

Picone, J. M., A. E. Hedin, D. P. Drob, and A. C. Aikin (2002), NRLMSISE-00 empirical model of the atmosphere: Statistical comparisons and scientific issues, *J. Geophys. Res.*, *107*(A12), 1468, doi:10.1029/2002JA009430.

Price, G. D., R. W. Smith, and G. Hernandez (1995), Simultaneous measurements of large vertical winds in the upper and lower thermosphere, *J. Atmos. Terr. Phys.*, *57*, 631.

Randall, C. E., et al. (2005), Stratospheric effects of energetic particle precipitation in 2003–2004, *Geophys. Res. Lett.*, *32*, L05802, doi:10.1029/2004GL022003.

Randall, C. E., V. L. Harvey, C. S. Singleton, P. F. Bernath, C. D. Boone, and J. U. Kozyra (2006), Enhanced $NO_x$ in 2006 linked to strong upper stratospheric Arctic vortex, *Geophys. Res. Lett.*, *33*, L18811, doi:10.1029/2006GL027160.

Richmond, A. D., E. C. Ridley, and R. G. Roble (1992), A Thermosphere/Ionosphere General Circulation Model with coupled electrodynamics, *Geophys. Res. Lett.*, *19*, 601.

Sætre, C., C. A. Barth, J. Stadsnes, N. Østgaard, S. M. Bailey, D. N. Baker, and J. W. Gjerloev (2006), Comparisons of electron energy deposition derived from observations of lower thermospheric nitric oxide and from X-ray bremsstrahlung measurements, *J. Geophys. Res.*, *111*, A04302, doi:10.1029/2005JA011391.

Siskind, D. E., C. A. Barth, D. S. Evans, and R. G. Roble (1989a), The response of thermospheric nitric oxide to an auroral storm: 2. Auroral latitudes, *J. Geophys. Res.*, *94*, 16,899.

Siskind, D. E., C. A. Barth, and R. G. Roble (1989b), The response of thermospheric nitric oxide to an auroral storm: 1. Low and middle latitudes, *J. Geophys. Res.*, *94*, 16,885.

Siskind, D. E., C. A. Barth, and J. M. Russel (1998), A climatology of nitric oxide in the mesosphere and thermosphere, *Adv. Space Res.*, *21*, 1353.

Solomon, S. C., and V. J. Abreu (1989), The 630-nm dayglow, *J. Geophys. Res.*, *94*, 6817.

Solomon, S. C., P. J. Crutzen, and R. G. Roble (1982), Photochemical coupling between the thermosphere and the lower atmosphere: 1. Odd nitrogen from 50 to 120 km, *J. Geophys. Res.*, *87*, 7206.

Solomon, S. C., P. B. Hays, and V. J. Abreu (1988), The auroral 6300 å emission: Observations and modeling, *J. Geophys. Res.*, *93*, 9867.

Solomon, S. C., S. M. Bailey, and T. N. Woods (2001), Effect of solar soft X-rays on the lower ionosphere, *Geophys. Res. Lett.*, *28*, 2149.

Stevens, M. H. (1995), Nitric oxide gamma band fluorescent scattering and selp-absorption: 1. The mesosphere and lower thermosphere, *J. Geophys. Res.*, *100*, 14,735.

Sugino, M., R. Fujii, S. Nozawa, S. C. Buchert, H. J. Opgenoorth, and A. Brekke (2002), Relative contribution of ionospheric conductivity and electric field to ionospheric current, *J. Geophys. Res.*, *107*(A10), 1330, doi:10.1029/2001JA007545.

Torr, M. R., et al. (1995), A far ultraviolet imager for the International Solar-Terrestrial physics mission, *Space Sci. Rev.*, *71*, 329.

S. M. Bailey, Department of Electrical and Computer Engineering, Virginia Polytechnic Institute and State University, Blacksburg, VA 24061-0111, USA.

D. N. Baker and C. A. Barth, Laboratory for Atmospheric and Space Physics, University of Colorado, Boulder, CO 80303-7814, USA.

G. A. Germany, Center for Space Plasma and Aeronomic Research, University of Alabama in Huntsville, Huntsville, AL 35899, USA.

J. W. Gjerloev, Johns Hopkins University Applied Physics Laboratory, Laurel, MD 20723-6099, USA.

N. Østgaard, C. Sætre, and J. Stadsnes, Department of Physics and Technology, University of Bergen, N-5007 Bergen, Norway. (camilla.satre@ift.uib.no)